MATERIALS CHEMISTRY FRONTIERS

RESEARCH ARTICLE

View Article Online
View Journal | View Issue

Cite this: *Mater. Chem. Front.*, 2021, **5**, 5130

Optimizing supramolecular fluorescent materials with responsive multi-color tunability toward soft biomimetic skins†

Muqing Si, ‡[ab] Huihui Shi,‡[ab] Hao Liu,[ab] Hui Shang,[a] Guangqiang Yin,[ab] Shuxin Wei,[ab] Shuangshuang Wu,[ab] Wei Lu *[ab] and Tao Chen *[ab]

Received 12th February 2021,
Accepted 24th April 2021

DOI: 10.1039/d1qm00248a

rsc.li/frontiers-materials

Many natural organisms have evolved to display responsive biofluorescence color changes that facilitate excellent environmental adaptability for camouflage, concealment, protection or signaling. Such interesting phenomena have inspired the development of various artificial fluorescence-color changeable materials with versatile uses, such as responsive displays, encryption, and sensing. However, it is challenging to replicate the dynamic fluorescence color camouflage capacities of living organisms by using soft synthetic materials, but such systems can work as soft biomimetic skins to enhance the function of certain machines (such as robots or prosthetics). Herein, we report a kind of robust supramolecular fluorescent soft material with both multi-color tunability and room-temperature self-healing features on the basis of synergistic multiple hydrogen bonding and dynamic lanthanide coordination interactions. Soft biomimetic camouflage and display skins were further demonstrated, which can be conformally worn on commercial robots to help them merge into different-colored environments or enable on-demand information display in response to a subtle interplay between several environmental stimuli (*e.g.*, humidity, metal ions). This work has made fluorescence color changeable biomimetic skins accessible and is expected to inspire the development of powerful fluorescent materials with as-not-yet-imaginable performance.

Introduction

Many natural organisms, including marine mollusks, fishes, butterflies, spiders and flowers, have evolved to display smart green, orange or red biofluorescence emission coloration, which results from the absorption of electromagnetic radiation (*e.g.*, high-energy blue or UV light).[1–4] These responsive biofluorescence color changes are reported to enable a number of natural creatures to achieve adaptive camouflage with concealment, protection, or signaling. Inspired by these phenomena, there have been many attempts to mimic such stimuli-triggered fluorescence-color changeable functions into artificial materials,[5–12] which have inspired the development of many promising systems with versatile uses in soft actuators,[13–15] sensing,[16–21] information encryption[22–31] and so on. For example, Tang[13] *et al.* physically incorporated a pH-responsive tetra-(4-pyridylphenyl)ethylene fluorophore into the crosslinked poly(acrylamide/sodium 4-styrene sulfonate) network to develop a bio-inspired bilayer hydrogel actuator, which displayed synergistic fluorescence color changes and complex shape deformation in response to environmental pH changes. Zhang[19] and coworkers reported powerful amine-responsive ratiometric fluorescent films that enable the visual detection of seafood freshness by covalently grafting fluorescein isothiocyanate as the indicator and protoporphyrin IX as the internal reference onto cellulose acetate polymer. Very recently, we have also presented a urease entrapped multi-responsive fluorescent hydrogel system, which can be used as a promising information encryption platform with unique self-destroying capacity after decryption when triggered by certain predesigned environmental stimuli.[25]

However, despite these impressive advances, the dynamic fluorescence color camouflage capacities of living organisms have not been replicated by using soft synthetic materials. But such systems are of great research importance because they can serve as soft biomimetic skins to enhance the function

[a] *Key Laboratory of Marine Materials and Related Technologies, Zhejiang Key Laboratory of Marine Materials and Protective Technologies, Ningbo Institute of Materials Technology and Engineering, Chinese Academy of Sciences, Ningbo 315201, China. E-mail: luwei@nimte.ac.cn, tao.chen@nimte.ac.cn*

[b] *School of Chemical Sciences, University of Chinese Academy of Sciences, Beijing 100049, China*

† Electronic supplementary information (ESI) available. See DOI: 10.1039/d1qm00248a

‡ These authors contributed equally to this work.

of certain machines (such as robots or prosthetics).[32] For instance, it would help commercial robots merge into various backgrounds by wearing such soft biomimetic skins with dynamic colors and patterns that can be programmed to be similar to the surrounding environments. Besides, a number of animals also utilize responsive fluorescence color changes as the display strategy for mating, hunting and communication in low- or no-light conditions. Such fluorescence-based display functions are also expected to be replicated in soft biomimetic skins for efficient human–machine interaction and visualization. Nevertheless, to the best of the authors' knowledge, the fabrication of fluorescence color changeable biomimetic skins still remains underdeveloped. One of the primary reasons is that the variation range of the fluorescence wavelength is usually narrow. Therefore, it is of great importance to develop robust fluorescent materials with programmable multi-state color switching behavior in response to environmental stimuli. Meanwhile, room-temperature self-healing and remolding properties are also desired for biomimetic skins in order to ensure the long-time service.[33–37]

Herein, we combined dynamic supramolecular hydrogen bonding and lanthanide coordination interactions[38–50] to construct smart supramolecular fluorescent materials with both multi-color tunability and room-temperature self-healing features, which can serve as powerful biomimetic skins to help commercial robots achieve the desirable camouflage/display functions. The materials were prepared by the supramolecular assembly of poly(*N*-(2-hydroxyethyl)acrylamide-*co*-methyl 6-(3-(2-(methacryloyloxy)ethyl)ureido)picolinate) (abbreviated as PHM) and poly(*N*-(2-hydroxyethyl) acrylamide-*co*-*N*-vinyl carbazole) (abbreviated as PHNVC), followed by coordination with Europium ions (Eu^{3+}). As illustrated in Scheme 1, the as-prepared Eu-PHNVC/PHM systems emit intense red fluorescence, but their emission color can be continuously programmed from red to green[51–53] and then to blue in response to the sequential stimuli of Terbium ions (Tb^{3+}) and environmental humidity.[54–59] In addition, owing to the highly dynamic and reversible nature of their supramolecular crosslinks, the developed materials are also endowed with satisfying room-temperature self-healing and remolding properties. On the basis of these appealing advantages, soft biomimetic camouflage or display skins were designed, which can be worn on commercial chameleon robots to help them merge into different-colored environment backgrounds or display the pre-coded information in response to environmental changes, just behaving like natural chameleons.

Results and discussion

The first step to construct the supramolecular fluorescent polymeric materials is the synthesis of a specially designed ligand monomer, methyl-6-((3-(2-methacryloyloxy)ethyl)ureido) picolinate (MAUP), which comprises both the urea group and the methyl picolinate group. MAUP was synthesized by an addition reaction between the isocyanate group of 2-isocyanatoethyl methacrylate and the amino group of 6-aminopyridine-2-carboxylate (Fig. S1, ESI†). Its chemical structure was clearly confirmed by ^{1}H, ^{13}C NMR, and ESI-MS spectroscopy (Fig. S2–S4, ESI†). Because of its strong and multiple intermolecular hydrogen bonds, MAUP could be dissolved in hot DMSO and DMF. It was then used for radical polymerization with *N*-(2-hydroxyethyl) acrylamide (HEAA) in hot DMSO to produce the targeted polymer, P(HEAA-*co*-MAUP) (PHM) (Fig. 1a). Limited by its moderate solubility in DMSO at 70 °C, the molar feed ratio of MAUP/HEAA is set as 1 : 21.2 in the synthetic experiment. According to its ^{1}H NMR spectrum (Fig. S5–S8 and Table S1, ESI†), the molar content of the MAUP moiety in the obtained PHM polymer was calculated to be 6.2 mol%, which is in agreement with the results calculated based on the UV-Vis spectrum (Fig. S9 and S10, ESI†).

The soft fluorescent polymeric materials were then prepared and studied. To do this, different mass ratios of PHM and Eu^{3+} nitrate were first mixed in DMF. The obtained PHM-Eu^{3+}/DMF solution was homogeneous and transparent under daylight. Subsequently, the mixed solution was decanted into a polytetrafluoroethylene (PTFE) mold to obtain the fluorescent polymeric film after evaporating DMF at 60 °C (Fig. 1a and Fig. S11, ESI†). The obtained Eu-PHM film was highly transparent under daylight, but exhibited bright red fluorescence, in contrast to the non-fluorescent PHM film (Fig. 1a and Fig. S12, ESI†). This observation clearly indicated the formation of fluorescent MAUP-Eu^{3+} coordination complexes, in which the MAUP ligand served as a sensitizer to largely enhance the red emission of Eu^{3+} through a known resonance energy transfer (RET) process. As is evidenced in Fig. S13 (ESI†), there were a series of characteristic narrow emission bands corresponding to the intra-$4f^6$ $^5D_0 \rightarrow {}^7F_{0-4}$ transitions of MAUP-Eu^{3+} complexes with a maximal emission wavelength at 617 nm ($^5D_0 \rightarrow {}^7F_2$) in the fluorescence spectrum of the Eu-PHM film. More direct evidence for the MAUP-Eu^{3+} coordination interactions came from the X-ray photoelectron spectra (XPS) of the Eu-PHM film and the PHM film (Fig. 1d and Fig. S14, S15, ESI†). The XPS N 1s spectrum of the PHM film is fitted with two components that can be assigned to the N atoms of the amide bond (N_1, 399.86 eV) and pyridine (N_2, 400.96 eV). However, the N 1s spectrum of the Eu-PHM film was deconvoluted into three peaks at 408.11, 401.21, and 400.06 eV, which correspond to the N atoms of pyridine (N_3*), the urea group on MAUP (N_2*), and the amide bond on HEAA (N_1*) (Fig. 1d and Fig. S14, ESI†). The XPS O 1s peak also shifted with the addition of Eu^{3+} (Fig. S15, ESI†). The obvious increase of the binding energy of N atoms in pyridine and the O atoms of O=C indicated that Eu^{3+} coordinates with MAUP by sharing an electron pair with these atoms. Besides, the split-up of the N_1 binding energy revealed a significant change of the chemical environment of N atoms in the urea group, which was caused by the formation of the MAUP-Eu^{3+} complex. Besides the red fluorescent Eu-PHM film, an intensely green fluorescent Tb-PHM film was also readily prepared from the DMF solution of PHM-Tb^{3+}. By further utilizing the Eu^{3+}/Tb^{3+} mixture to coordinate with the PHM polymer, soft multicolor fluorescent Eu/Tb-PHM films were then obtained, for which the emission

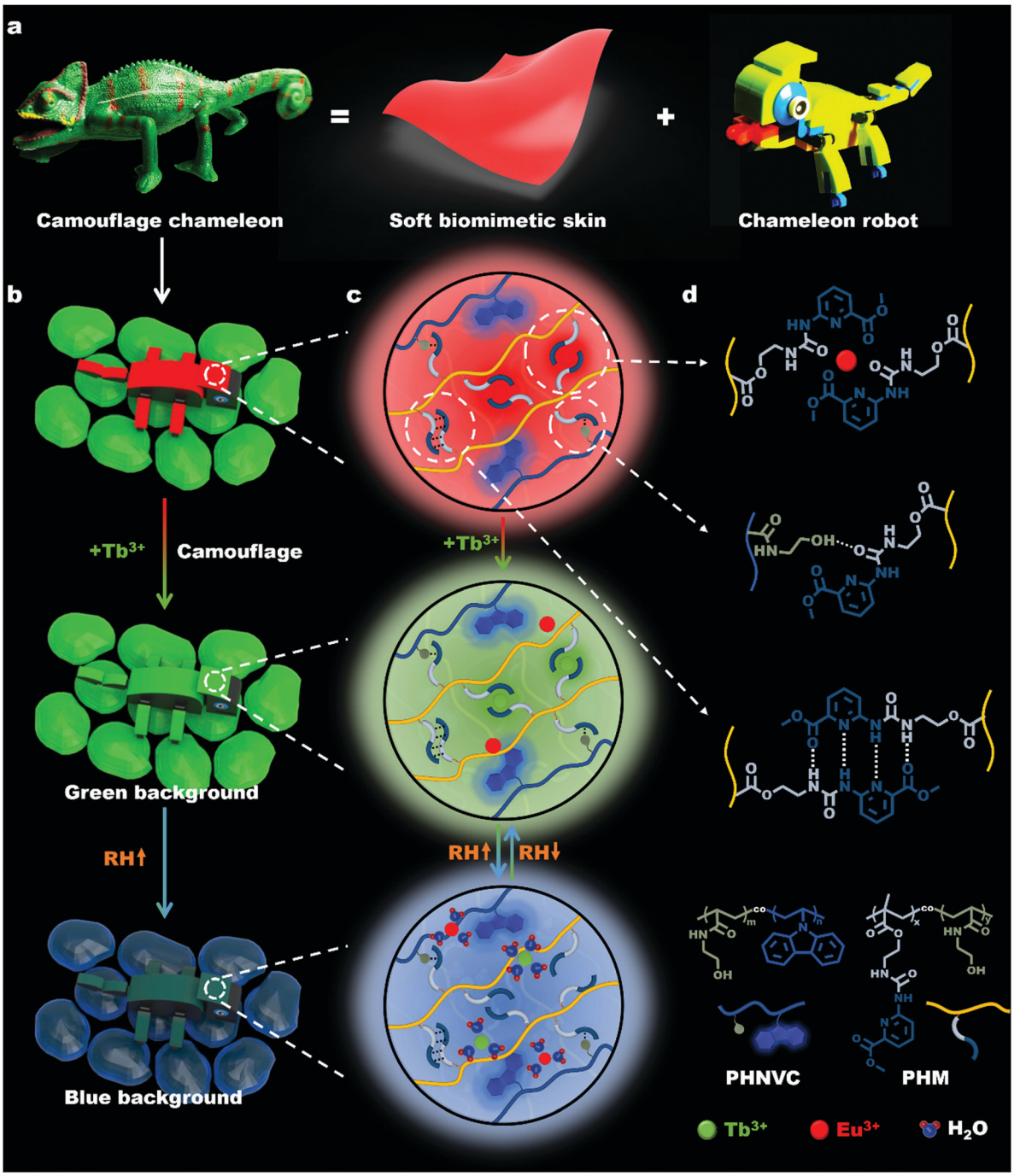

Scheme 1 Schematic illustration of the soft supramolecular fluorescent film with programmable full-color tunability. (a) Illustration of the process of wearing a soft biomimetic camouflage skin on a commercial chameleon robot to obtain a camouflage chameleon. (b) Schemes showing its ability to merge into green and blue environment backgrounds in response to sequential environmental changes (*e.g.*, Tb^{3+} ions, humidity). Illustration of (c) the mechanism of full-color tunability and (d) the involved supramolecular interactions. Relative humidity (RH) is the percentage of actual water vapor in the air as a percentage of saturated humidity at the experimental temperature (20 °C).

color could be facilely modulated by varying the Eu^{3+}/Tb^{3+} molar ratio (Fig. 1c). As shown in Fig. 1b, upon decreasing the Eu^{3+}/Tb^{3+} molar ratio, the fluorescence intensity of the green band at 547 nm increased at the cost of the fluorescence intensity of the red band at 617 nm.

Interestingly, the red emission of the Eu-PHM film was very sensitive to environmental moisture. As summarized in Fig. 1e, its fluorescence intensity was found to decrease sharply as the ambient humidity increased. For example, its peak intensity at 617 nm dropped by 76% when elevating the environmental relative humidity from 11% to 98%. This unique moisture-triggered fluorescence quenching was ascribed to the stepwise dissociation of MAUP-Eu^{3+} coordination interactions in the presence of water (Fig. 1a). As is well known, such lanthanide

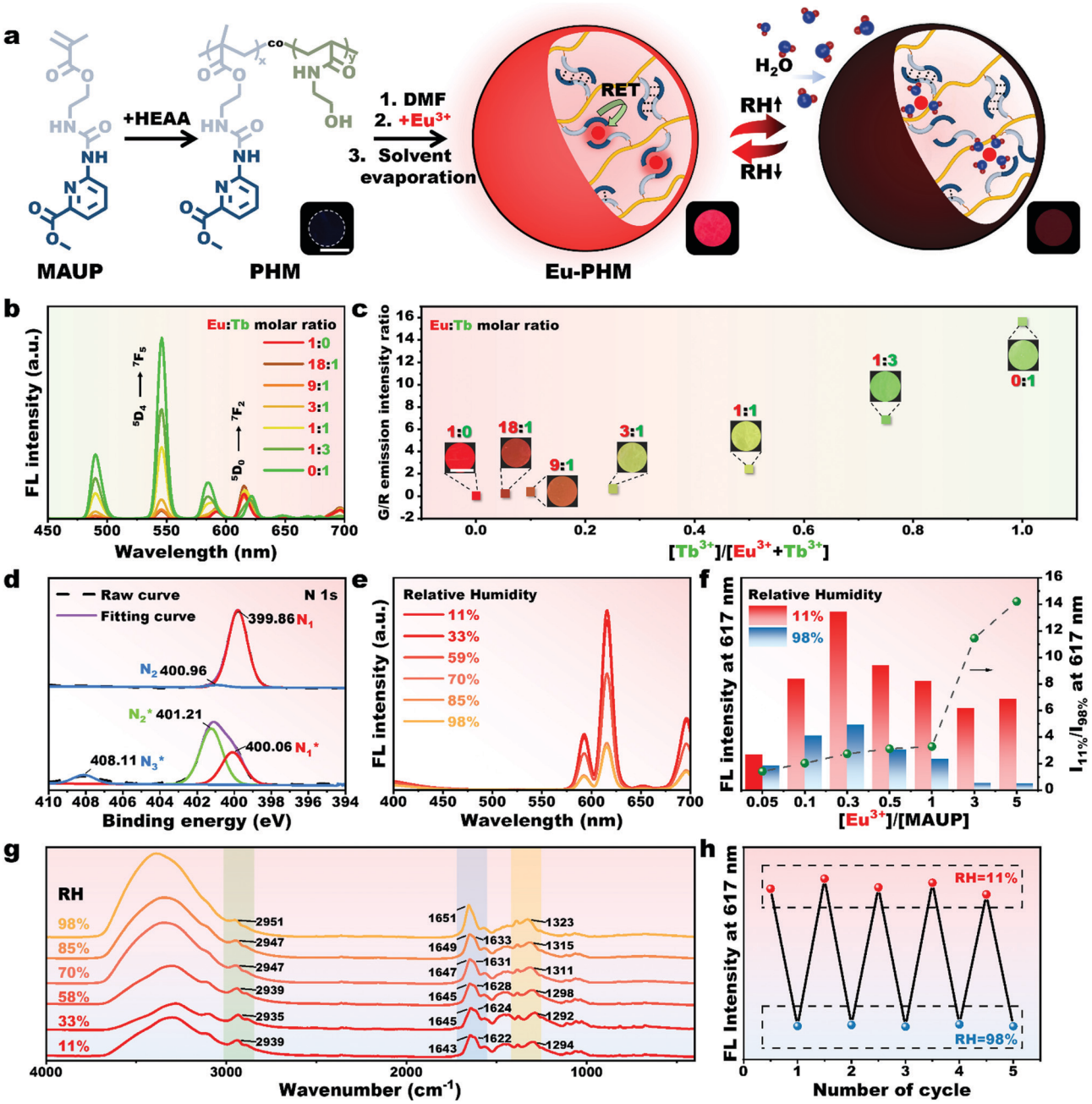

Fig. 1 (a) Schematic illustration showing the preparation of Eu-PHM and its humidity-dependent fluorescence reduction. (b) Fluorescence spectra (λ_{ex} = 254 nm) of multi-color fluorescent Eu/Tb-PHM films. (c) The green/red (G/R) emission intensity ratio as a function of the Eu^{3+}/Tb^{3+} molar ratio (1 : 0, 18 : 1, 9 : 1, 3 : 1, 1 : 1, 1 : 3, 0 : 1) and the corresponding photographs. All photos were taken under a 254 nm UV lamp. (d) High-resolution XPS fitting results for N 1s of PHM and Eu-PHM. (e) The fluorescence spectra of Eu-PHM recorded at different humidities (λ_{ex} = 254 nm). (f) The peak fluorescence intensities of the Eu-PHM films with different Eu^{3+}/MAUP ratios at 617 nm, which were recorded at RH = 11% and RH = 98%. (g) ATR-FTIR spectra of the Eu-PHM film (Eu^{3+}/MAUP = 5 : 1) at different relative humidities. (h) Cyclic peak intensity changes of the Eu-PHM film at 617 nm by alternately varying the environmental humidity.

ions as Eu^{3+} show more affinity to O atoms in comparison with N atoms according to Hard–Soft–Acid–Base theory. Therefore, the large amount of free water molecules in the surrounding environment might compete with the pyridine binding sites of the MAUP ligand, leading to the breakage of pyridine-Eu^{3+} coordination bonds and thus largely blocked energy transfer from the ligand to central Eu^{3+} ions. Further studies revealed that the Eu-PHM film with a higher Eu^{3+}/MAUP ratio was more sensitive to humidity changes. Fig. 1f and Fig. S16 (ESI†) summarize their fluorescence quenching ratios ($I_{11\%}/I_{98\%}$) at 617 nm as a function of the Eu^{3+}/ligand ratio ($I_{11\%}$ represents the fluorescence intensity at RH = 11%, $I_{98\%}$ represents the fluorescence intensity at RH = 98%). When the Eu^{3+}/ligand ratio was below 1, $I_{11\%}/I_{98\%}$ was relatively small. But the $I_{11\%}/I_{98\%}$

value quickly increased to 14.2 in the presence of excess Eu^{3+} (the Eu^{3+}/MAUP molar ratio of 5 : 1). This phenomenon is easily understood because the Eu^{3+} ions with lower coordination numbers contain more unoccupied coordination sites and thus they more easily coordinate with the free water molecules in the air. Therefore, the polymeric film with a Eu^{3+}/MAUP molar ratio of 5 : 1 was chosen as the example in the following studies. To gain a better understanding of the humidity-dependent fluorescence quenching, attenuated total reflection Fourier transform infrared (ATR-FTIR) spectroscopy of the Eu-PHM film was then conducted. As shown in Fig. 1g, at a low RH (11%), the Eu-PHM film shows characteristic peaks at 1294 cm^{-1}, 1643 cm^{-1}, 1622 cm^{-1} and 2939 cm^{-1}, which are attributed to the stretching vibrations of the C–O–C, the C═O of ester groups, the C═O of urea groups and the C–H of pyridine, respectively. As humidity increased, the peaks

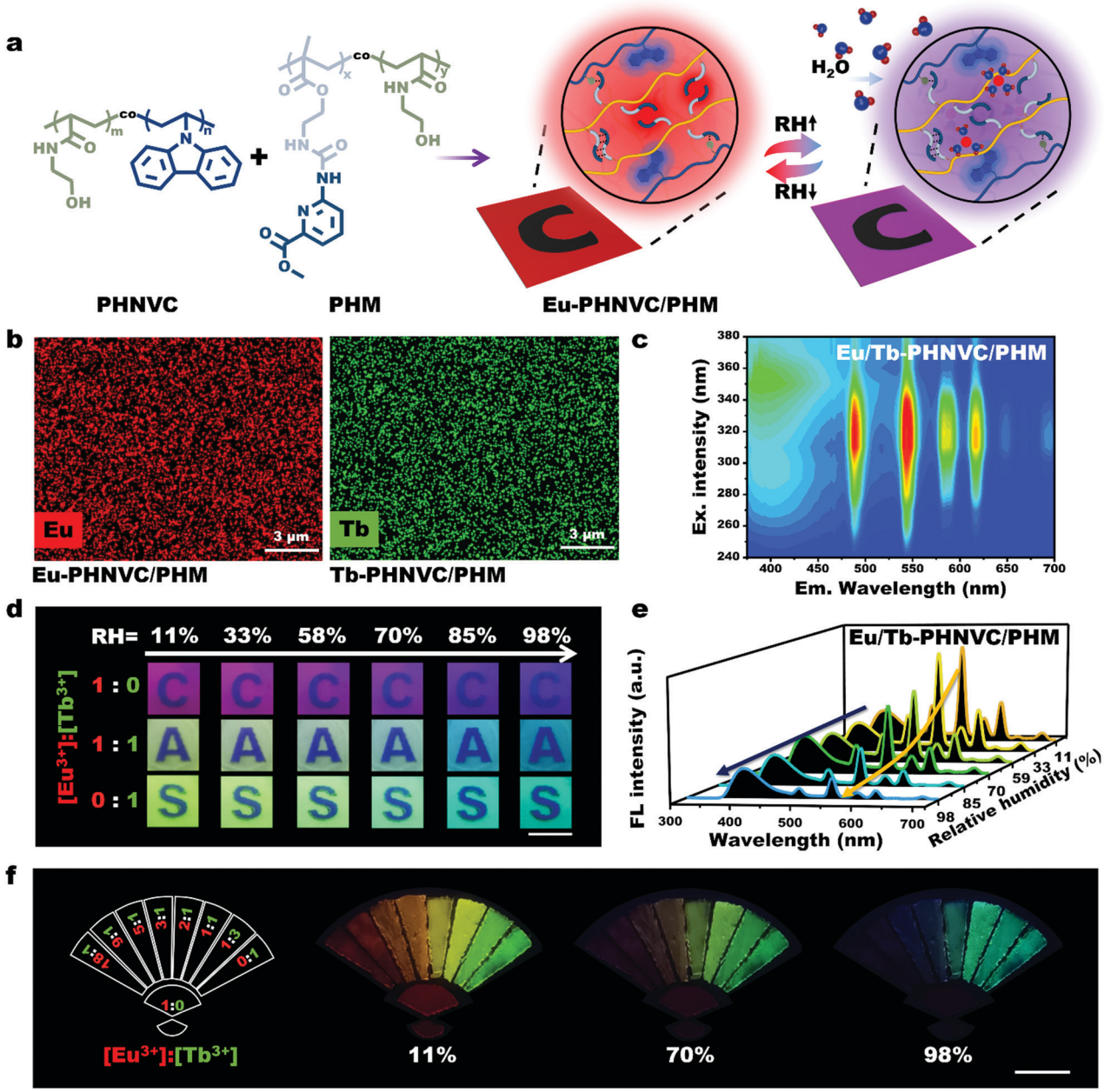

Fig. 2 Humidity-sensitive color changing ability of the Eu/Tb-PHNVC/PHM films. (a) Molecular structures of PHM and PHNVC, as well as the schematic illustration of the formation of Eu-PHNVC/PHM through supramolecular interactions. (b) Energy dispersive X-ray spectroscopy (EDS) mapping of Eu in the Eu-PHNVC/PHM film and Tb in the Tb-PHNVC/PHM film. (c) Excitation-fluorescence mapping of the Eu/Tb-PHNVC/PHM film (Eu^{3+}/Tb^{3+} = 1 : 1) under ambient conditions. Digital photos showing (d) the emission color change process of several Eu/Tb-PHNVC/PHM films as humidity varies (scale bar: 5 mm) and (e) the fluorescence spectral changes of one typical sample Eu/Tb-PHNVC/PHM film (Eu^{3+}/Tb^{3+} = 1 : 1) (λ_{ex} = 254 nm). (f) Extensive illustration of the humidity-sensitive color changing ability of Eu/Tb-PHNVC/PHM (scale bar: 5 mm). All of the photographs were taken under a 254 nm UV lamp.

mentioned above moved to higher wavenumbers, which implied the dissociation of the coordination bond between MAUP and Eu^{3+}. Similarly, the multicolor Eu/Tb-PHM films also exhibited an interesting humidity-triggered fluorescence intensity reduction property. Fig. S17 (ESI†) compares their fluorescence images recorded at different RHs, which gradually faded with increasing environmental humidity. Note that the observed humidity-responsive fluorescence response is highly reversible, as evidenced by the result that the peak intensity change of the Eu-PHM film at 617 nm could be repeated for many cycles by alternately varying the environmental humidity (Fig. 1h). However, owing to their close chemical structures, the MAUP-Eu^{3+} and MAUP-Tb^{3+} complexes displayed nearly the same fluorescence quenching kinetics in response to the environmental humidity stimulus. Consequently, no noticeable emission color change upon humidity change was observed for these flexible multicolor fluorescent Eu/Tb-PHM films (Fig. S18, ESI†).

For achieving the remarkable humidity-triggered emission color change, a non-responsive blue-light-emitting P(HEAA-NVC) (PHNVC) polymer was further synthesized and co-assembled into the Eu/Tb-PHM films. The blue fluorescent PHNVC polymer was produced by the radical polymerization of *N*-(2-hydroxyethyl)acrylamide and N-vinylcarbazole and characterized by ^{1}H NMR spectroscopy (Fig. 2a and Fig. S19–S21, ESI†). According to its UV-Vis spectrum, the content of vinylcarbazole in the obtained polymer was calculated to be 14.3 mol% (Fig. S22 and S23, ESI†). The blue fluorescence of this carbazole-grafted PHNVC polymer was proved to be unaffected by the environmental humidity change (Fig. S24, ESI†). The solvent evaporation process of the PHNVC/PHM-Eu^{3+}/DMF solution induces supramolecular crosslinks between these polymer chains *via* hydrogen bonds, resulting in the formation of transparent soft polymeric films with micron thickness (Fig. S25 and S26, ESI†). The O-/N-containing groups (*e.g.*, –C═O, –NH, –OH) grafted on these PHNVC and PHM polymer chains form high-density hydrogen bonds between them, making these luminogens stably and evenly distributed in the film matrix, as evidenced by the energy dispersive X-ray spectroscopy (EDS) mapping images (Fig. 2b and Fig. S27, ESI†). To produce the remarkable humidity-triggered emission color change, the content of PHNVC in the fluorescent polymeric films was optimized to be 30.1 wt% (Fig. S28, ESI†). The excitation-fluorescence mapping of Eu/Tb-PHNVC/PHM revealed the simultaneous fluorescence emission of three distinct luminogens, that is, the carbazole, MAUP-Tb^{3+} and MAUP-Eu^{3+}, respectively (Fig. 2c). As shown in Fig. 2d, the optimized Eu-PHNVC/PHM film appeared purple-red under 254 nm UV light irradiation, but gradually changed to purple as humidity increased. A similar humidity-triggered emission color change was further observed for Tb-PHNVC/PHM and Eu/Tb-PHNVC/PHM (Eu^{3+}/Tb^{3+} = 1 : 1) films, which displayed green-to-cyan and yellow-to-blue color changes, respectively. These results were consistent with their corresponding fluorescence spectra recorded at different humidities (Fig. 2e and Fig. S29, ESI†). Specifically, both the red (around 617 nm) and green (around 547 nm) emission bands gradually decreased, while the blue fluorescence band around 402 nm remained nearly unchanged. In a more extensive color changing display, a colorful folding fan made up of nine Eu/Tb-PHNVC/PHM films with different Eu^{3+}/Tb^{3+} ratios was fabricated, which could switch from a warm-toned one into a cold-toned one, accompanying rising humidity (Fig. 2f).

Except for humidity, other stimuli like acid/base chemicals, light, and temperature could also trigger similar red-to-blue (or green-to-blue) fluorescence color change of the Eu/Tb-PHNVC/PHM films (Fig. S30–S32, ESI†). Further, more interesting red-to-green fluorescence-color change of the Eu-PHNVC/PHM film was further demonstrated by employing Tb^{3+} as a stimulus (Fig. 3a). As demonstrated in Fig. 3b, after locally spraying different amounts of Tb^{3+} ions onto certain regions of the Eu^{3+}-doped red fluorescent zebra, some of its stripes and the tail were transformed into yellow, orange and green, respectively, producing a colorful zebra. This is because the Eu^{3+} ions in the red fluorescent MAUP-Eu^{3+} complexes could be gradually replaced by the addition of excess Tb^{3+}, resulting in the formation of green fluorescent MAUP-Tb^{3+} complexes in the films. As expected, the initial red color of the zebra was proved to be regained after the re-addition of Eu^{3+}/methanol solution (0.25 M). These results indicated that the emission color of the obtained polymeric films could be reversibly switched between red and green by employing Tb^{3+} or Eu^{3+} as a stimulus (Fig. S33, ESI†).

Having demonstrated both the humidity-responsive red-to-purple and Tb^{3+}-triggered red-to-green fluorescence color change, we next explored the possibility to achieve the programmable multi-state color switching behavior over nearly the full color gamut. To this end, one square-shaped Eu-PHNVC/PHM film with purple-red fluorescence color was exposed to the sequential stimuli of humidity and Tb^{3+}. As demonstrated in Fig. 3c, the fluorescence color of the film could be continuously programmed from purple-red to blue and green, nearly covering the full visible spectrum. Importantly, each color shown in this array can be stably kept through the precise control of environmental humidity and concentration of the added Tb^{3+}. Remarkably, the re-addition of Eu^{3+} onto the film was capable of gradually reversing this multi-state color change process. These results suggest the possibility that the emission color of the obtained Eu-PHNVC/PHM film could be reversibly switched between nearly any two colors in response to the subtle interplay between the humidity and Tb^{3+} stimuli.

Having discovered the multi-color tunability achieved by the MAUP-Eu^{3+}/Tb^{3+} complex, we further explore other important features endowed by these supramolecular interactions. The mechanical studies indicate that the tensile strength, Young's modulus, and elongation at break of the Eu-PHM/PHNVC sample (thickness ~ 30 μm) are 3.89 MPa, 50.91 MPa, and 45%, respectively (Fig. S34, ESI†). Nanomechanical mapping with an atomic force microscope (AFM) (Fig. S35, ESI†) reveals the presence of both hydrogen bonds and metal complexation crosslinks, which further endowed the Eu-PHNVC/PHM films with other noteworthy features, including their self-healing and

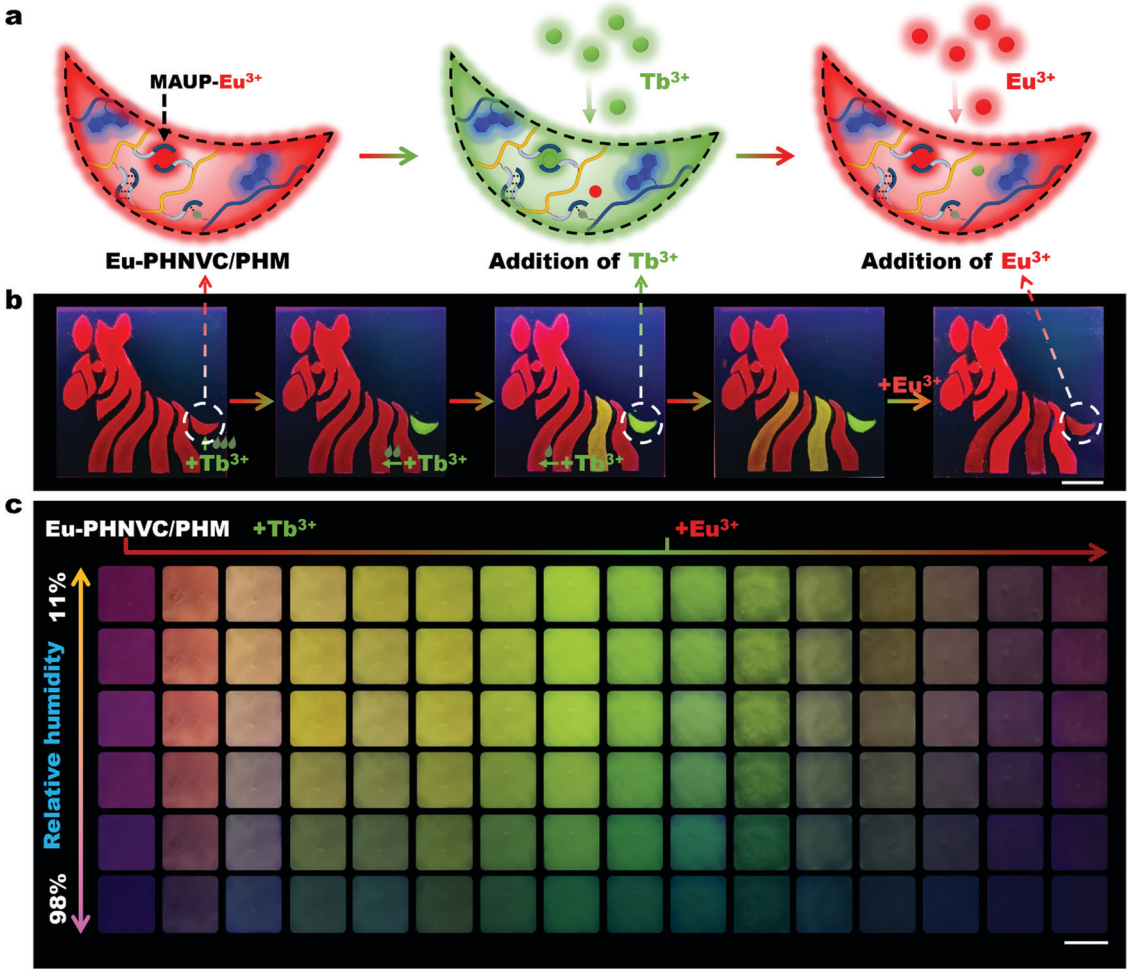

Fig. 3 The programmable full-color tunable behavior of the Eu-PHNVC/PHM film. (a) Schematic illustration of the color changing process triggered by the sequential addition of Eu^{3+} and Tb^{3+}. (b) Digital photos showing the process of producing a colorful zebra by locally spraying different amounts of $Tb(NO_3)_3$/methanol solution onto certain regions (scale bar: 10 mm). (c) Digital photos showing the programmable full-color tunable process of the Eu-PHNVC/PHM film in response to the subtle interplay between humidity and Tb^{3+} (scale bar: 5 mm). All of the photographs were taken under a 254 nm UV lamp.

remolding properties. As shown in Fig. 4a and Fig. S36 (ESI†), two pieces of broken films can self-heal into an integral rectangular piece at room temperature when placed in contact and placed in a high humidity environment (98%) for 4 h. It should be noted that the self-healing process was not observed in normal humidity (*e.g.*, RH ~ 60%) for even 24 h (Fig. S37, ESI†), indicating that high humidity is essential to promote the self-healing process. This is because both the hydrogen bonds and MAUP-Eu^{3+} coordination bonds became more dynamic in the presence of high-concentration water molecules in a high humidity environment. More dynamic supramolecular interactions also pose less restrictions on the polymer chains, which promote the penetration of the polymer chains into each other on the edges. After the film was brought back to the normal environment (*e.g.*, RH ~ 60%), new hydrogen bonds and MAUP-Eu^{3+} coordination bonds form between the polymer chains and sew the broken pieces together. The healed film was sufficiently stable to resist external forces (Movie S1, ESI†). Furthermore, the shape of the fluorescent films was capable of being changed through remolding (Fig. 4b). In a typical experiment, the fragments of Eu-PHNVC/PHM films were first collected and dissolved completely in DMF. A new homogeneous film with a certain shape would then be obtained after transferring the solution into a mold and evaporating the solvent. This remolding process can be repeated several times owing to the absence of chemical crosslinks. Interestingly, if Tb^{3+} was added during the film remolding process, the reset of both film shape and color could be achieved simultaneously, which has not been achieved previously.

On the basis of these satisfying self-healing and color-changing properties, one blossoming flower was further constructed by self-healing five red fluorescent petals with one blue fluorescent stamen (Fig. 4c). Note that the petals were composed of the Eu-PHNVC/PHM film with responsive multicolor change behavior, while the stamen was made from filter paper. Consequently, one bio-inspired fluorescent flower was obtained, the color of which could be regulated over a large color gamut in response to the subtle interplay between the humidity and Tb^{3+} stimuli.

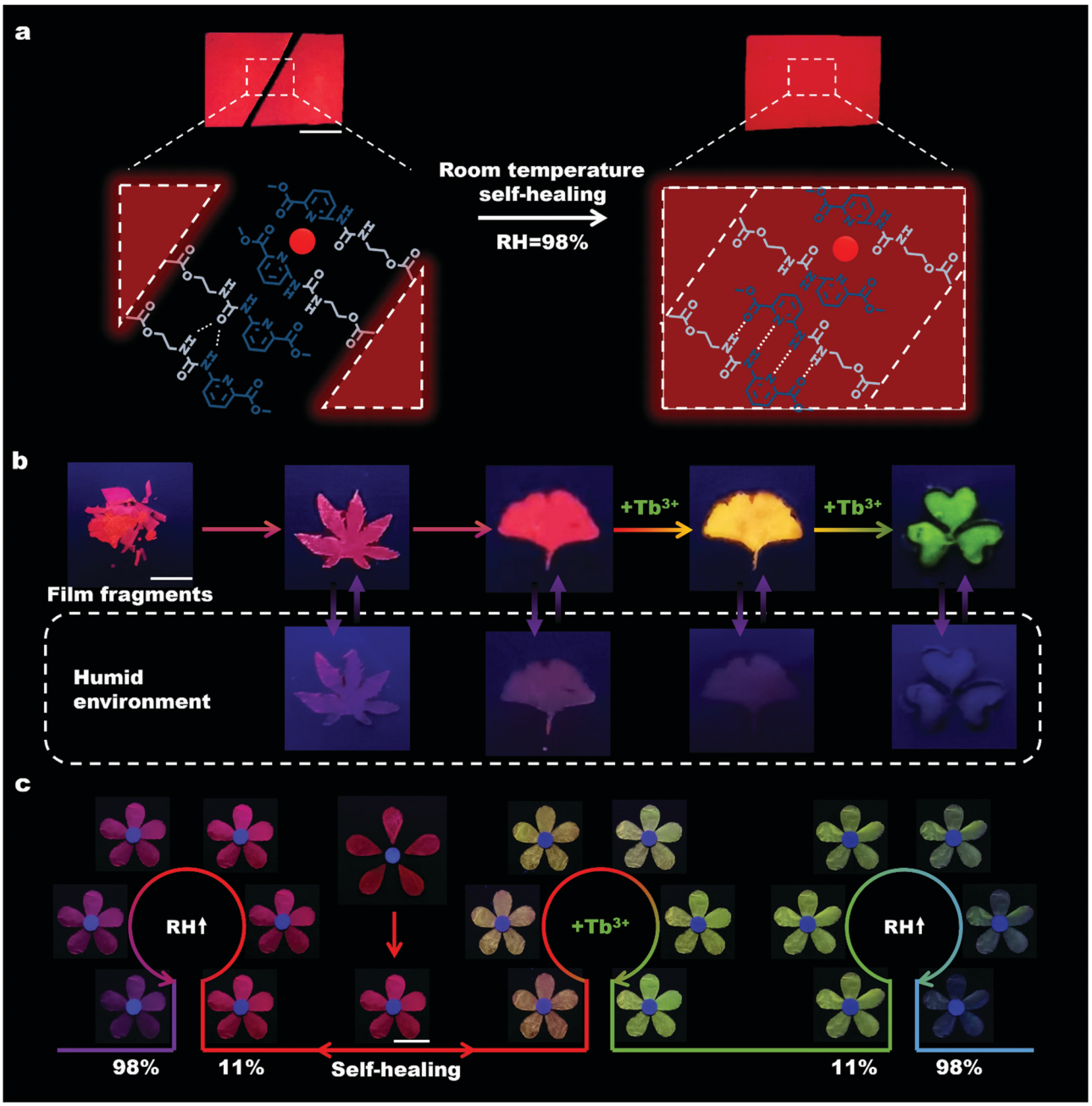

Fig. 4 Self-healing and remolding properties of the Eu-PHNVC/PHM film. (a) Digital photos showing the self-healing process of the Eu-PHNVC/PHM film and the proposed mechanism (scale bar: 5 mm). (b) Digital photos showing the reset of both the shape and color of an Eu-PHNVC/PHM film (scale bar: 3 mm). (c) Digital photos of a self-healed flower and its full-spectrum color changing process in response to the subtle interplay between the humidity and Tb^{3+} stimuli (scale bar: 5 mm). All of the photographs were taken under a 254 nm UV lamp.

In addition to the flower, many natural animals also have evolved intriguing color changing ability for communication, reproduction or even camouflage in order to adapt to the environment. For example, *morpho* butterflies are well known for their beautiful iridescent wings, which can display dazzling color pattern changes in response to environmental variations (*e.g.*, humidity).[60] This interesting natural phenomenon encouraged us to design and fabricate their man-made counterparts (Fig. 5a and Fig. S38, ESI†). To this end, we designed and prepared an artificial butterfly by self-healing two red-colored wings made of the Eu-PHNVC/PHM film and one blue-colored body made of filter paper together. Behaving like a natural *morpho* butterfly, this fluorescent butterfly gradually adjusted its wing color from red to yellow, green and then cyan, corresponding to the cascading changes (Tb^{3+} concentration increase, followed by a subsequent humidity increase) in the surrounding environment. By a combination of self-healing and multicolor-changing properties, the dazzling and colorful pattern change of the *morpho* butterfly was also mimicked by using the flexible multicolor systems (Fig. S39, ESI†).

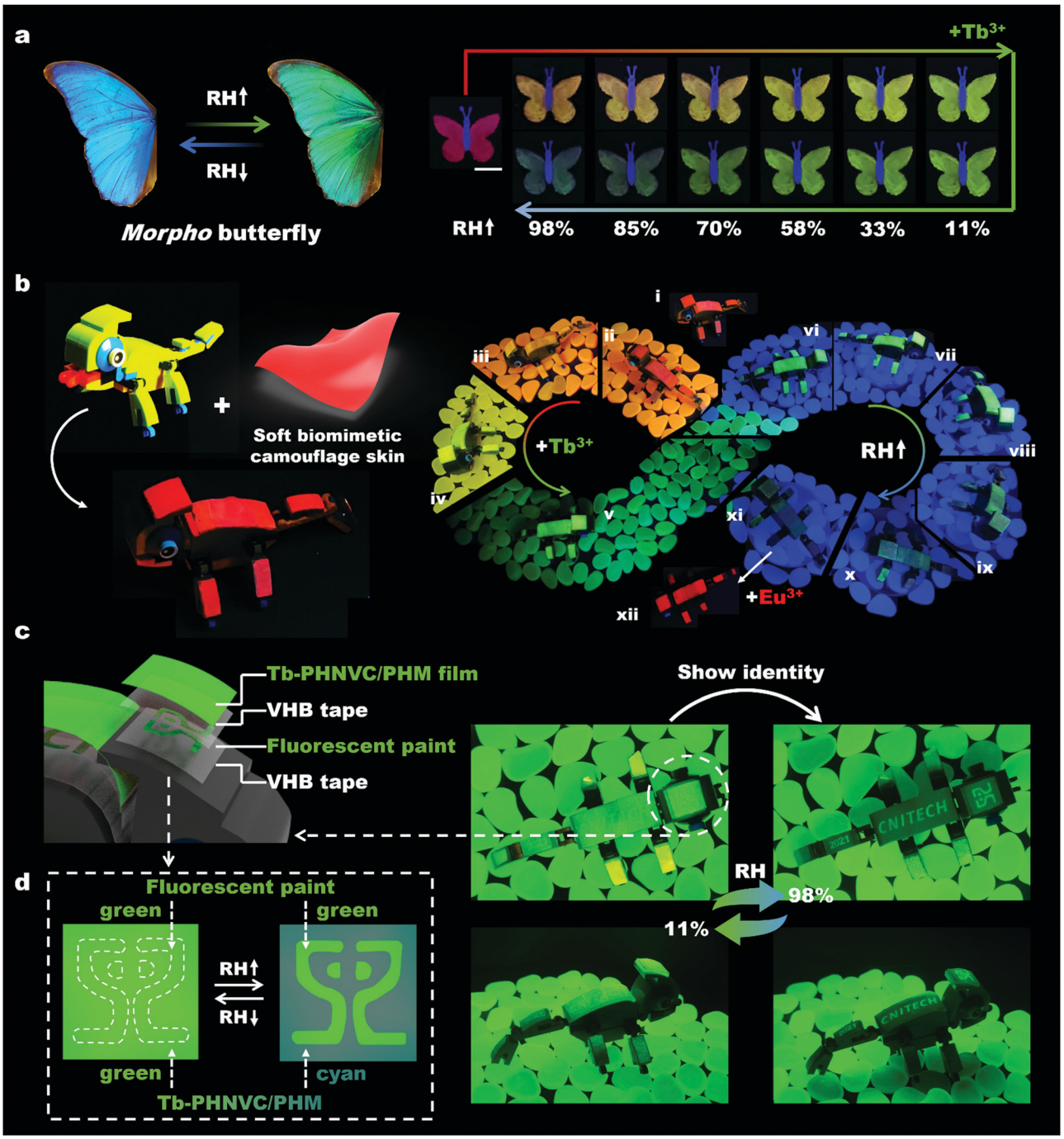

Fig. 5 Application as the soft biomimetic skins. (a) Photos showing the bio-inspired color-changing process of an artificial butterfly based on the Eu-PHNVC/PHM films in response to the sequential stimuli of Tb^{3+} and humidity (scale bar: 5 mm). (b) Photos showing the chameleon robot wearing the soft biomimetic camouflage skin and the camouflage process into different colored backgrounds. (c and d) Schematic illustration of the soft biomimetic display skin that can help the decorated chameleon robot facilely switch between the camouflage mode and the display mode upon environmental humidity changes. All of the photographs were taken under a 254 nm UV lamp.

Chameleon is another master of color manipulation which has excellent control over its skin colors for the sake of camouflage upon environmental changes. In an attempt to mimic this fascinating function into artificial systems, we utilized the Eu-PHNVC/PHM films with programmable full-color tunability to produce powerful biomimetic skins that can help the commercial robots achieve the desirable camouflaging behavior, that is, to adapt its body color to match the background in order to conceal itself. As shown in Fig. 5b, a commercial chameleon robot that has a static yellow color under daylight and cannot change its color was employed as an example. Surprisingly, after decorating the tailored

Eu-PHNVC/PHM-based soft biomimetic skin onto its surface using a very high bonding (VHB) tape, a smart robot with bio-inspired camouflage ability was achieved. At the initial state, the decorated robot displayed red skin color, which can be easily observed against the orange background. After spraying Tb^{3+}/methanol solution into the surrounding environment, the color of the decorated biomimetic skin quickly changed to orange, which made the robot merge into the background. Using similar methods, this decorated robot can be programmed to match yellow or green backgrounds. Furthermore, when combined with the stimulus of environmental humidity change, it was also capable of dynamically camouflaging into blue backgrounds. Furthermore, the developed soft biomimetic skins can also be engineered to help commercial robots realize the on-demand display function. As shown in Fig. 5c, the biomimetic display skins were fabricated by layer-by-layer integration of the Tb-PHNVC/PHM film, VHB tape and the green luminous paint with pre-coded information. As a consequence, the camouflage mode of the decorated chameleon robot could be facilely switched to the display mode upon environmental humidity changes. This is because the decorated chameleon robot displayed intense green emission that is similar to the background (the camouflage mode) at a low environmental humidity, while at a high environmental humidity the green emission of the Tb-PHNVC/PHM film was largely quenched, making the pre-coded information of the luminous paint layer become quite visible to show its identity (the display mode) (Fig. 5d and Fig. S40, ESI†). In this way, we preliminarily demonstrated that our supramolecular fluorescent system with full-color tunability could potentially serve as efficient biomimetic skins that assist the robots to accomplish the desirable camouflage or display tasks in complex natural environments.

Conclusions

In conclusion, we first reported multi-color tunable fluorescent materials with room-temperature self-healing properties and further demonstrated their potential to serve as soft biomimetic camouflage/display skins that could enhance the functions of commercial robots. The materials are produced by the supramolecular assembly of the responsive lanthanide coordinated fluorescent Eu-PHM polymer and the non-responsive blue fluorescent carbazole-functionalized PHNVC polymer *via* multiple hydrogen bonds. They are characterized by satisfying room-temperature self-healing ability, as well as Tb^{3+}-triggered red-to-green emission color change and subsequently humidity-responsive green-to-blue emission color change. Based on the synergistic effect of these self-healing and multi-color tunable properties, robust biomimetic camouflage and display skins are demonstrated, which could potentially help commercial robots merge into different-colored surroundings or enable on-demand information display. The proposed strategy holds great potential to make the desirable camouflage/display robots accessible and is also expected to inspire the future development of more powerful fluorescence color-changing materials with versatile applications in bio-inspired soft robotics, visual display/detection, smart camouflage and so on.

Author contributions

M. Si and H. Shi contributed equally to this work. Specifically, M. Si, H. Shi, W. Lu, and T. Chen conceived and designed the experiments. M. Si, H. Shi, H. Liu, H. Shang, and S. Wu performed the investigation. G. Yin and S. Wei contributed to characterization, analysis, and discussion. M. Si, H. Shi, and W. Lu cowrote the paper.

Conflicts of interest

There are no conflicts to declare.

Acknowledgements

This research was supported by the National Natural Science Foundation of China (Grant No. 21774138, 51773215), the Key Research Program of Frontier Sciences, Chinese Academy of Sciences (QYZDB-SSW-SLH036), and the Youth Innovation Promotion Association of Chinese Academy of Sciences (2019297), K. C. Wong Education Foundation (GJTD-2019-13).

Notes and references

1 G. Lee, M. Kong, D. Park, J. Park and U. Jeong, Electro-Photoluminescence Color Change for Deformable Visual Encryption, *Adv. Mater.*, 2020, **32**, 1907477.
2 A. Salih, A. Larkum, G. Cox, M. Kuhl and O. Hoegh-Guldberg, Fluorescent pigments in corals are photoprotective, *Nature*, 2000, **408**, 850–853.
3 J. S. Sparks, R. C. Schelly, W. L. Smith, M. P. Davis, D. Tchernov, V. A. Pieribone and D. F. Gruber, The covert world of fish biofluorescence: a phylogenetically widespread and henotypically variable phenomenon, *PLoS One*, 2014, **9**, 83259.
4 E. A. Widder, Bioluminescence in the ocean: origins of biological, chemical, and ecological diversity, *Science*, 2010, **328**, 704–708.
5 C. Calvino, A. Guha, C. Weder and S. Schrettl, Self-Calibrating Mechanochromic Fluorescent Polymers Based on Encapsulated Excimer-Forming Dyes, *Adv. Mater.*, 2018, **30**, 1704603.
6 H. Chen, F. Yang, Q. Chen and J. Zheng, A Novel Design of Multi-Mechanoresponsive and Mechanically Strong Hydrogels, *Adv. Mater.*, 2017, **29**, 1606900.
7 D. Kim, J. E. Kwon and S. Y. Park, Fully Reversible Multistate Fluorescence Switching: Organogel System Consisting of Luminescent Cyanostilbene and Turn-On Diarylethene, *Adv. Funct. Mater.*, 2018, **28**, 1706213.

8 M. Li, Q. Zhang, Y. N. Zhou and S. Zhu, Let spiropyran help polymers feel force!, *Prog. Polym. Sci.*, 2018, **79**, 26–39.
9 R. Merindol, G. Delechiave, L. Heinen, L. H. Catalani and A. Walther, Modular Design of Programmable Mechanofluorescent DNA Hydrogels, *Nat. Commun.*, 2019, **10**, 528.
10 J. Shin, J. H. Kyhm, A. R. Hong, J. D. Song, K. Lee, H. Ko and H. S. Jang, Multicolor Tunable Upconversion Luminescence from Sensitized Seed-Mediated Grown LiGdF4:Yb,Tm-Based Core/Triple-Shell Nanophosphors for Transparent Displays, *Chem. Mater.*, 2018, **30**, 8457–8464.
11 R. Sun, S. Feng, D. Wang and H. Liu, Fluorescence-Tuned Silicone Elastomers for Multicolored Ultraviolet Light-Emitting Diodes: Realizing the Processability of Polyhedral Oligomeric Silsesquioxane-Based Hybrid Porous Polymers, *Chem. Mater.*, 2018, **30**, 6370–6376.
12 S. Wei, Z. Li, W. Lu, H. Liu, J. Zhang, T. Chen and B. Z. Tang, Multicolor Fluorescent Polymeric Hydrogels, *Angew. Chem., Int. Ed.*, 2021, **60**, 8608.
13 Z. Li, P. Liu, X. Ji, J. Gong, Y. Hu, W. Wu, X. Wang, H. Q. Peng, R. T. K. Kwok, J. W. Y. Lam, J. Lu and B. Z. Tang, Bioinspired Simultaneous Changes in Fluorescence Color, Brightness, and Shape of Hydrogels Enabled by AIEgens, *Adv. Mater.*, 2020, **32**, 1906493.
14 C. Ma, W. Lu, X. Yang, J. He, X. Le, L. Wang, J. Zhang, M. J. Serpe, Y. Huang and T. Chen, Bioinspired Anisotropic Hydrogel Actuators with On-Off Switchable and Color-Tunable Fluorescence Behaviors, *Adv. Funct. Mater.*, 2018, **28**, 1704568.
15 S. Wei, W. Lu, X. Le, C. Ma, H. Lin, B. Wu, J. Zhang, P. Theato and T. Chen, Bioinspired Synergistic Fluorescence-Color-Switchable Polymeric Hydrogel Actuators, *Angew. Chem., Int. Ed.*, 2019, **58**, 16243–16251.
16 K. Benson, A. Ghimire, A. Pattammattel and C. V. Kumar, Protein Biophosphors: Biodegradable, Multifunctional, Protein-Based Hydrogel for White Emission, Sensing, and pH Detection, *Adv. Funct. Mater.*, 2017, **27**, 1702955.
17 J. Hai, T. Li, J. Su, W. Liu, Y. Ju, B. Wang and Y. Hou, Reversible Response of Luminescent Terbium(III)-Nanocellulose Hydrogels to Anions for Latent Fingerprint Detection and Encryption, *Angew. Chem., Int. Ed.*, 2018, **57**, 6786–6790.
18 G. He, N. Yan, J. Yang, H. Wang, L. Ding, S. Yin and Y. Fang, Pyrene-Containing Conjugated Polymer-Based Fluorescent Films for Highly Sensitive and Selective Sensing of TNT in Aqueous Medium, *Macromolecules*, 2011, **44**, 4759–4766.
19 R. Jia, W. Tian, H. Bai, J. Zhang, S. Wang and J. Zhang, Amine-responsive cellulose-based ratiometric fluorescent materials for real-time and visual detection of shrimp and crab freshness, *Nat. Commun.*, 2019, **10**, 795.
20 Y. Jiang and N. Hadjichristidis, Diels-Alder Polymer Networks with Temperature-Reversible Cross-Linking-Induced Emission, *Angew. Chem., Int. Ed.*, 2021, **60**, 331–337.
21 H. S. Jung, P. Verwilst, W. Y. Kim and J. S. Kim, Fluorescent and colorimetric sensors for the detection of humidity or water content, *Chem. Soc. Rev.*, 2016, **45**, 1242–1256.
22 L. Gu, H. Wu, H. Ma, W. Ye, W. Jia, H. Wang, H. Chen, N. Zhang, D. Wang, C. Qian, Z. An, W. Huang and Y. Zhao, Color-tunable ultralong organic room temperature phosphorescence from a multicomponent copolymer, *Nat. Commun.*, 2020, **11**, 944.
23 J. Ji, D. Hu, J. Yuan and Y. Wei, An Adaptable Cryptosystem Enabled by Synergies of Luminogens with Aggregation-Induced-Emission Character, *Adv. Mater.*, 2020, **32**, 2004616.
24 X. Ji, R. T. Wu, L. Long, X. S. Ke, C. Guo, Y. J. Ghang, V. M. Lynch, F. Huang and J. L. Sessler, Encoding, Reading, and Transforming Information Using Multifluorescent Supramolecular Polymeric Hydrogels, *Adv. Mater.*, 2018, **30**, 1705480.
25 X. Le, H. Shang, H. Yan, J. Zhang, W. Lu, M. Liu, L. Wang, G. Lu, Q. Xue and T. Chen, Spatiotemporal regulation of fluorescence in a urease-embedded hydrogel for multistage information security, *Angew. Chem., Int. Ed.*, 2021, **60**, 3640.
26 F. Li, X. Wang, Z. Xia, C. Pan and Q. Liu, Photoluminescence Tuning in Stretchable PDMS Film Grafted Doped Core/Multishell Quantum Dots for Anticounterfeiting, *Adv. Funct. Mater.*, 2017, **27**, 1700051.
27 Z. Li, H. Chen, B. Li, Y. Xie, X. Gong, X. Liu, H. Li and Y. Zhao, Photoresponsive Luminescent Polymeric Hydrogels for Reversible Information Encryption and Decryption, *Adv. Sci.*, 2019, **6**, 1901529.
28 T. Ma, T. Li, L. Zhou, X. Ma, J. Yin and X. Jiang, Dynamic wrinkling pattern exhibiting tunable fluorescence for anticounterfeiting applications, *Nat. Commun.*, 2020, **11**, 1811.
29 H. Wang, X. Ji, Z. Li, C. N. Zhu, X. Yang, T. Li, Z. L. Wu and F. Huang, Preparation of a white-light-emitting fluorescent supramolecular polymer gel with a single chromophore and use of the gel to fabricate a protected quick response code, *Mater. Chem. Front.*, 2017, **1**, 167–171.
30 S. Zeng, D. Zhang, W. Huang, Z. Wang, S. G. Freire, X. Yu, A. T. Smith, E. Y. Huang, H. Nguon and L. Sun, Bio-inspired sensitive and reversible mechanochromisms via strain-dependent cracks and folds, *Nat. Commun.*, 2016, **7**, 11802.
31 Y. Zhang, X. Le, Y. Jian, W. Lu, J. Zhang and T. Chen, 3D Fluorescent Hydrogel Origami for Multistage Data Security Protection, *Adv. Funct. Mater.*, 2019, **29**, 1905514.
32 S. A. Morin, R. F. Shepherd, S. W. Kwok, A. A. Stokes, A. Nemiroski and G. M. Whitesides, Camouflage and Display for Soft Machines, *Science*, 2012, **337**, 828–832.
33 S. Bhattacharya, R. S. Phatake, S. Nabha Barnea, N. Zerby, J. J. Zhu, R. Shikler, N. G. Lemcoff and R. Jelinek, Fluorescent Self-Healing Carbon Dot/Polymer Gels, *ACS Nano*, 2019, **13**, 1433–1442.
34 Y. Deng, Q. Zhang, B. L. Feringa, H. Tian and D. H. Qu, Toughening a Self-Healable Supramolecular Polymer by Ionic Cluster-Enhanced Iron-Carboxylate Complexes, *Angew. Chem., Int. Ed.*, 2020, **59**, 5278–5283.
35 Z. Jiang, M. L. Tan, M. Taheri, Q. Yan, T. Tsuzuki, M. G. Gardiner, B. Diggle and L. A. Connal, Strong, Self-Healable, and Recyclable Visible-Light-Responsive Hydrogel Actuators, *Angew. Chem., Int. Ed.*, 2020, **59**, 7049–7056.
36 Z. Li, Z. Hou, H. Fan and H. Li, Organic-Inorganic Hierarchical Self-Assembly into Robust Luminescent Supramolecular Hydrogel, *Adv. Funct. Mater.*, 2017, **27**, 1604379.

37 Q. Rong, W. Lei, L. Chen, Y. Yin, J. Zhou and M. Liu, Anti-freezing, Conductive Self-healing Organohydrogels with Stable Strain-Sensitivity at Subzero Temperatures, *Angew. Chem., Int. Ed.*, 2017, **56**, 14159–14163.

38 B. Li, C. L. Lin, C. J. Lu, J. J. Zhang, T. He, H. Y. Qiu and S. C. Yin, A rapid and reversible thermochromic supramolecular polymer hydrogel and its application in protected quick response codes, *Mater. Chem. Front.*, 2020, **4**, 869–874.

39 B. Li, T. He, X. Shen, D. T. Tang and S. C. Yin, Fluorescent supramolecular polymers with aggregation induced emission properties, *Polym. Chem.*, 2019, **10**, 796–818.

40 Q. M. Zhang, W. Xu and M. J. Serpe, Optical devices constructed from multiresponsive microgels, *Angew. Chem., Int. Ed.*, 2014, **53**, 4827–4831.

41 C. Xie, W. Sun, H. Lu, A. Kretzschmann, J. Liu, M. Wagner, H. J. Butt, X. Deng and S. Wu, Reconfiguring surface functions using visible-light-controlled metal-ligand coordination, *Nat. Commun.*, 2018, **9**, 3842.

42 H. Wang, X. Ji, Z. Li and F. Huang, Fluorescent Supramolecular Polymeric Materials, *Adv. Mater.*, 2017, **29**, 1606117.

43 Y. Ma, P. She, K. Y. Zhang, H. Yang, Y. Qin, Z. Xu, S. Liu, Q. Zhao and W. Huang, Dynamic metal-ligand coordination for multicolour and water-jet rewritable paper, *Nat. Commun.*, 2018, **9**, 3.

44 W. Lu, X. Le, J. Zhang, Y. Huang and T. Chen, Supramolecular shape memory hydrogels: a new bridge between stimuli-responsive polymers and supramolecular chemistry, *Chem. Soc. Rev.*, 2017, **46**, 1284–1294.

45 Q. Li, J. Hu, J. Lv, X. Wang, S. Shao, L. Wang, X. Jing and F. Wang, Through-Space Charge-Transfer Polynorbornenes with Fixed and Controllable Spatial Alignment of Donor and Acceptor for High-Efficiency Blue Thermally Activated Delayed Fluorescence, *Angew. Chem., Int. Ed.*, 2020, **59**, 20174–20182.

46 J. Li, J. Wang, H. Li, N. Song, D. Wang and B. Z. Tang, Supramolecular materials based on AIE luminogens (AIEgens): construction and applications, *Chem. Soc. Rev.*, 2020, **49**, 1144–1172.

47 A. Lavrenova, D. W. Balkenende, Y. Sagara, S. Schrettl, Y. C. Simon and C. Weder, Mechano- and Thermoresponsive Photoluminescent Supramolecular Polymer, *J. Am. Chem. Soc.*, 2017, **139**, 4302–4305.

48 Z. Huang and X. Ma, Tailoring Tunable Luminescence via Supramolecular Assembly Strategies, *Cell Rep. Phys. Sci.*, 2020, **1**, 1–26.

49 L. Hu, Q. Zhang, X. Li and M. J. Serpe, Stimuli-responsive polymers for sensing and actuation, *Mater. Horiz.*, 2019, **6**, 1774–1793.

50 Y. Z. Chang, Y. Chen and Y. Liu, Multicolor luminescent supramolecular hydrogels based on cucurbit[8]uril and OPV derivative, *Soft Matter*, 2019, **15**, 9881–9885.

51 P. Chen, Q. Li, S. Grindy and N. Holten-Andersen, White-Light-Emitting Lanthanide Metallogels with Tunable Luminescence and Reversible Stimuli-Responsive Properties, *J. Am. Chem. Soc.*, 2015, **137**, 11590–11593.

52 J. Wang, S. Sun, B. Wu, L. Hou, P. Ding, X. Guo, M. A. Cohen Stuart and J. Wang, Processable and Luminescent Supramolecular Hydrogels from Complex Coacervation of Polycations with Lanthanide Coordination Polyanions, *Macromolecules*, 2019, **52**, 8643–8650.

53 K. Meng, C. Yao, Q. Ma, Z. Xue, Y. Du, W. Liu and D. Yang, A Reversibly Responsive Fluorochromic Hydrogel Based on Lanthanide-Mannose Complex, *Adv. Sci.*, 2019, **6**, 1802112.

54 Y. Cheng, J. Wang, Z. Qiu, X. Zheng, N. L. C. Leung, J. W. Y. Lam and B. Z. Tang, Multiscale Humidity Visualization by Environmentally Sensitive Fluorescent Molecular Rotors, *Adv. Mater.*, 2017, **29**, 1703900.

55 Y. Jiang, Y. Cheng, S. Liu, H. Zhang, X. Zheng, M. Chen, M. Khorloo, H. Xiang, B. Z. Tang and M. Zhu, Solid-state intramolecular motions in continuous fibers driven by ambient humidity for fluorescent sensors, *Natl. Sci. Rev.*, 2021, **8**, nwaa135.

56 M. Li, Q. Lyu, L. Sun, B. Peng, L. Zhang and J. Zhu, Fluorescent Metallosupramolecular Elastomers for Fast and Ultrasensitive Humidity Sensing, *ACS Appl. Mater. Interfaces*, 2020, **12**, 39665–39673.

57 Y. Yao, C. Yin, S. Hong, H. Chen, Q. Shi, J. Wang, X. Lu and N. Zhou, Lanthanide-Ion-Coordinated Supramolecular Hydrogel Inks for 3D Printed Full-Color Luminescence and Opacity-Tuning Soft Actuators, *Chem. Mater.*, 2020, **32**, 8868–8876.

58 L. Zhang and P. Naumov, Light- and Humidity-Induced Motion of an Acidochromic Film, *Angew. Chem., Int. Ed.*, 2015, **54**, 8642–8647.

59 X. Zhou, L. Wang, Z. Wei, G. Weng and J. He, An Adaptable Tough Elastomer with Moisture-Triggered Switchable Mechanical and Fluorescent Properties, *Adv. Funct. Mater.*, 2019, **29**, 1903543.

60 R. A. Potyrailo, H. Ghiradella, A. Vertiatchikh, K. Dovidenko, J. R. Cournoyer and E. Olson, Morpho butterfly wing scales demonstrate highly selective vapour response, *Nat. Photonics*, 2007, **1**, 123–128.